Supporting Information

Defect chemistry of mixed ionic-electronic conductors under light: halide perovskites as master example

Davide Moia,* Joachim Maier

Max Planck Institute for Solid State Research, Heisenbergstraße 1, 70569 Stuttgart, Germany

*moia.davide@gmail.com
Current address: Fluxim AG, Katharina-Sulzer-Platz 2, 8400 Winterthur, Switzerland

Table of Contents

1. Model description and input parameters for calculations

In Scheme 1, we outline the equations (1—6) required to solve the model presented in the main text, along with approximated equations (indicated with ~) that can be used to obtain simplified solutions.

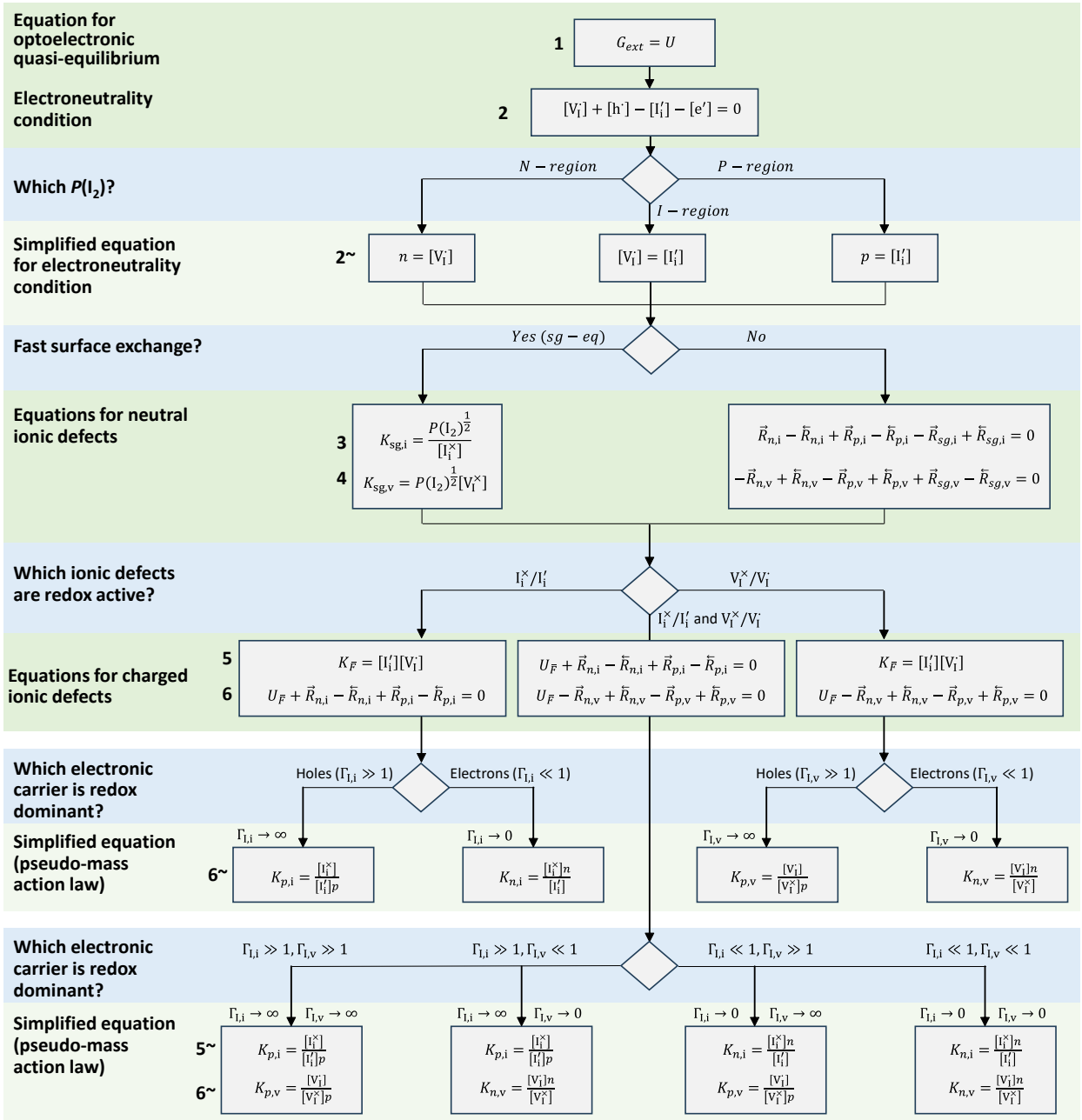

Scheme 1. Equations 1—6 used in the model described in the main text to analyze the defect chemistry of a mixed conductor (MAPI in this case) under light, for the different situations considered. Equations indicated with ~ are approximations to the general case. Equations 5~ and 6~ in the two redox active ionic defects case represent situations where the dominant redox reactions are essentially at equilibrium also under light.

The full list of input parameters used for the calculation shown in Figure 3 in the main text are shown in Table S1. The same parameters are used in all calculations unless stated otherwise.

Table S1. List of input parameters used in the calculations presented in the main text and in this document, unless stated otherwise.

N_C	$10^{19} cm^{-3}$	K_F	$10^{32} cm^{-6}$
N_V	$10^{19} cm^{-3}$	$K_{sg,i}$	$10^{-19} bar^{1/2} cm^3$
E_g	$1.63\ eV$	$K_{sg,v}$	$4.38 \times 10^{-5} bar^{1/2} cm^{-3}$
n_i	$2.1 \times 10^5 cm^{-3}$	$K_{p,i}$	$10^{-14} cm^3$
k_{rad}	$10^{-11} cm^{-3} s^{-1}$	$K_{n,v}$	$10^{14} cm^3$
τ_n	$2\ \mu s$	$P(I_2)_{IP}$	$10^{-2}\ bar$
τ_p	$2\ \mu s$	$P(I_2)_{NI}$	1.92×10^{-45}
$n_1 = p_1$	$2.1 \times 10^5 cm^{-3}$	$P(I_2)_i$	4.38×10^{-24}
$\gamma_n = \gamma_p$	$10^{-28} cm^{-6} s^{-1}$	$\vec{k}_F$	$10^{-15} cm^{-3} s^{-1}$
$E_C - E_{T,i}$	$0.2979\ eV$	$\vec{k}_{sg,v}$	$10^{24}\ cm^{-3} s^{-1}$
$E_{T,v} - E_V$	$0.2979\ eV$	$\vec{k}_{sg,i}$	$4.78\ 10^{16} s^{-1}$

Electronic properties:

- Representative values for bandgap energy and recombination rate constants and lifetimes for MAPI are used (see for example Ref.[1,2])

Ionic properties:

- The value for the anti-Frenkel disorder $K_F = 10^{32} cm^{-6}$ implies a concentration of defects (vacancies and interstitials) in the intrinsic region of $[I_i^{'}] = [V_I^{\cdot}] = 10^{16} cm^{-3}$. We note that estimates for the vacancy concentration in MAPI vary in literature, some studies pointing to significantly larger values ($10^{17} - 10^{19}\ cm^{-3}$).[3,4] We show calculation using a lower value to obtain better numerical convergence. The results in the main text and in this document are qualitatively relevant also to cases with larger defect concentrations.
- The value of $\vec{k}_F$ is estimated based on Equation 9, using a value of $r_F = 1\ nm$ and $D_F = 8 \times 10^{-10} cm^{-2} s^{-1}$
- $E_C - E_{T,i}$ and $E_{T,v} - E_V$ are the energetic distance of the redox levels for interstitials and vacancies from the conduction band minimum and valence band maximum, respectively. These values are used in the model to define $K_{sg,i}$ and $K_{sg,v}$ (see Table 1 in the main text). $K_{sg,i}$ and $K_{sg,v}$ can be calculated at $P(I_2)_i$, considering a value for $[I_i^{'}]$ and $[V_I^{\cdot}]$ of $\sqrt{K_F}$.

Solid-gas exchange:

- The values of $K_{sg,i}$ and $K_{sg,v}$ are selected assuming a trap energy level about 0.3 eV from the band edge for both interstitial (w.r.t. valence band edge) and vacancy defects (w.r.t. conduction band).

The value of $P(I_2)_{IP}$ and $P(I_2)_{NI}$ refer to the iodine partial pressure separating the intrinsic and the P region, and the iodine partial pressure separating the N and the intrinsic region, respectively, on the Kröger-Vink diagram for the equilibrium data. The value of $P(I_2)_{IP}$ is estimated from typical conductivity and mobility values for MAPI. The value of $P(I_2)_{NI}$ is obtained from $P(I_2)_{IP}$, n_i and K_F.

2. Redox activity and Shockley-Read-Hall analysis of redox active mobile ions

When dealing with charged ionic defects, the redox activity of at least one of such defects is a prerequisite for the solid-gas exchange reaction to take place and for evaluating defect chemical properties as a function of component chemical potential. It is indeed the reaction(s) dealing with the component (ion+electron) that connect the ionic and the electronic "worlds" and that mediate optoionic effects from nominally optoelectronic excitations.

Other situations involving redox inactive ionic defects could be of interest:

- Should the charged defects be redox inactive, the mixed conductor's stoichiometry would be fixed at the sample preparation stage. In the simplest case of no other ionic reactions other than the defect pair disorder reaction, the defect concentration would not be expected to vary upon illumination, as the ionic and the electronic behavior are decoupled.
- In situations far less common in ionic materials, the relevant defects may be redox inactive while also being neutrally charged. In this case, their equilibration with the gas phase would still be allowed. Yet, the lack of any direct or indirect interaction with the electronic charges would once again rule out any (first order) ionic effect upon illumination
- Beyond the field of ionic materials in the traditional sense, other demonstrations of ionic effects induced by illumination include systems where photo-induced electron transfer reactions between different phases occurs. In these cases, despite the lack of explicit reactions between ions and electrons, changes in ionic properties (e.g. ion concentrations) may be observed (due to e.g. electroneutrality, changes in material conformation etc.), and are often discussed in terms of "optoionic" effects.[5]

Shockley-Read-Hall analysis of redox active mobile ions

We refer to the reactions (*n*,i), (*p*,i) in the main text, reported here in Table S1.

Table S1. Redox reactions involving electrons or holes and iodine interstitial defects.

Redox (interstitial)	$I_i^{'} + h^{\cdot} \rightleftarrows I_i^{\times}$ (p,i)	$\vec{R}_{p,i} = \vec{k}_{p,i}\left[I_i^{'}\right]p$ $\overleftarrow{R}_{p,i} = \overleftarrow{k}_{p,i}\left[I_i^{\times}\right]$	$K_{p,i} = \dfrac{\left[I_i^{\times}\right]_{eq}}{\left[I_i^{'}\right]_{eq}p_{eq}}$
	$I_i^{'} \rightleftarrows I_i^{\times} + e^{'}$ (n,i)	$\vec{R}_{n,i} = \vec{k}_{n,i}\left[I_i^{'}\right]$ $\overleftarrow{R}_{n,i} = \overleftarrow{k}_{n,i}\left[I_i^{\times}\right]n$	$K_{n,i} = \dfrac{\left[I_i^{\times}\right]_{eq}n_{eq}}{\left[I_i^{'}\right]_{eq}} = K_{p,i}K_B$

Following the approach in Ref.[6] we can interpret the Shockley-Read-Hall rate based on the rate constants in Table S1. It follows that

$$U_I = \frac{np - n_i^2}{\tau_{n,i}(p + p_{1,i}) + \tau_p(n + n_{1,i})} \quad \text{(S1)}$$

where

$$\tau_{n,i} = \left[\vec{k}_{n,i}\left(\left[I_i^{\times}\right] + \left[I_i^{'}\right]\right)\right]^{-1} = \frac{n_{eq}\left[I_i^{\times}\right]_{eq}}{\vec{k}_{n,i}\left(\left[I_i^{\times}\right] + \left[I_i^{'}\right]\right)\left[I_i^{'}\right]_{eq}} \quad \text{(S2)}$$

$$\tau_{p,i} = \left[\vec{k}_{p,i}\left(\left[I_i^{\times}\right] + \left[I_i^{'}\right]\right)\right]^{-1}. \quad \text{(S3)}$$

The parameter $\Gamma_{I,i}$ is defined in the main text as the ratio of the forward rate for the (*n*,i) and (*p*,i) reactions ($\Gamma_{I,i} = \vec{R}_{p,i}/\vec{R}_{n,i}$) evaluated at $P(I_2) = P(I_2)_i$ at equilibrium.

It follows that $\Gamma_{I,i} = \vec{k}_{p,i}n_i/\vec{k}_{n,i}$. By rearranging the expressions for the capture time constants above, we obtain:

$$\Gamma_{I,i} = \frac{\tau_{n,i}}{\tau_{p,i}}\left.\frac{\left[I_i^{'}\right]}{\left[I_i^{\times}\right]}\right|_i \quad \text{(S4)}$$

Where $\left.\frac{\left[I_i^{'}\right]}{\left[I_i^{\times}\right]}\right|_i$ is the ratio of the iodide and iodine interstitial concentrations evaluated at $P(I_2)_i$ and at equilibrium. Based on the Fermi-Dirac statistics that establishes the relative concentration of the negative (occupied by an electron) and neutral interstitial defect (unoccupied), we can therefore write

$$\left.\frac{\left[I_i^{'}\right]}{\left[I_i^{\times}\right]}\right|_i = e^{-\frac{E_{T,i} - E_i}{k_B T}}, \quad \text{(S5)}$$

where the intrinsic energy $E_i = \frac{E_C + E_V}{2} + \frac{k_B T}{2} ln\left[\frac{N_V}{N_C}\right]$ and $E_{T,i}$ is the interstitial trap energy associated with the $I_i^{\times}/I_i^{'}$ redox.

Because $p_{1,i} = N_V e^{\frac{E_V - E_{T,i}}{k_B T}}$ and $n_{1,i} = N_C e^{-\frac{E_C - E_{T,i}}{k_B T}}$, we obtain:

$$\Gamma_{I,i} = \frac{\tau_{n,i}}{\tau_{p,i}}\sqrt{\frac{p_{1,i}}{n_{1,i}}}. \quad \text{(S6)}$$

A similar treatment can be applied to $\Gamma_{I,v}$ which also leads to an expression of the parameter h_{ion} based on the trapping parameters associated with the redox active mobile ions

$$\Gamma_{I,v} = \frac{\tau_{n,v}}{\tau_{p,v}}\sqrt{\frac{p_{1,v}}{n_{1,v}}} \quad \text{(S7)}$$

$$h_{ion} = \log_{10}\left(\frac{\tau_{n,v}\tau_{p,i}}{\tau_{p,v}\tau_{n,i}}\sqrt{\frac{p_{1,v}n_{1,v}}{p_{1,i}n_{1,i}}}\right) \quad \text{(S8)}$$

Finally, as mentioned in the main text, the parameters $\Gamma_{p,i}$ and $\Gamma_{n,v}$ are defined to parameterize the rate of hole trapping by an iodide interstitial and electron trapping by an iodide vacancy. Such rates are normalized by the radiative recombination rate, all rates being evaluated at equilibrium and for $P(I_2) = P(I_2)_i$. Their values can therefore be expressed as:

$$\Gamma_{p,i} = \frac{\vec{k}_{p,i}\sqrt{K_F}}{k_{rad} n_i} \qquad \text{(S9)}$$

$$\Gamma_{n,v} = \frac{\vec{k}_{n,v}\sqrt{K_F}}{k_{rad} n_i} \; . \qquad \text{(S10)}$$

3. Discussion of the quasi-equilibrium under light

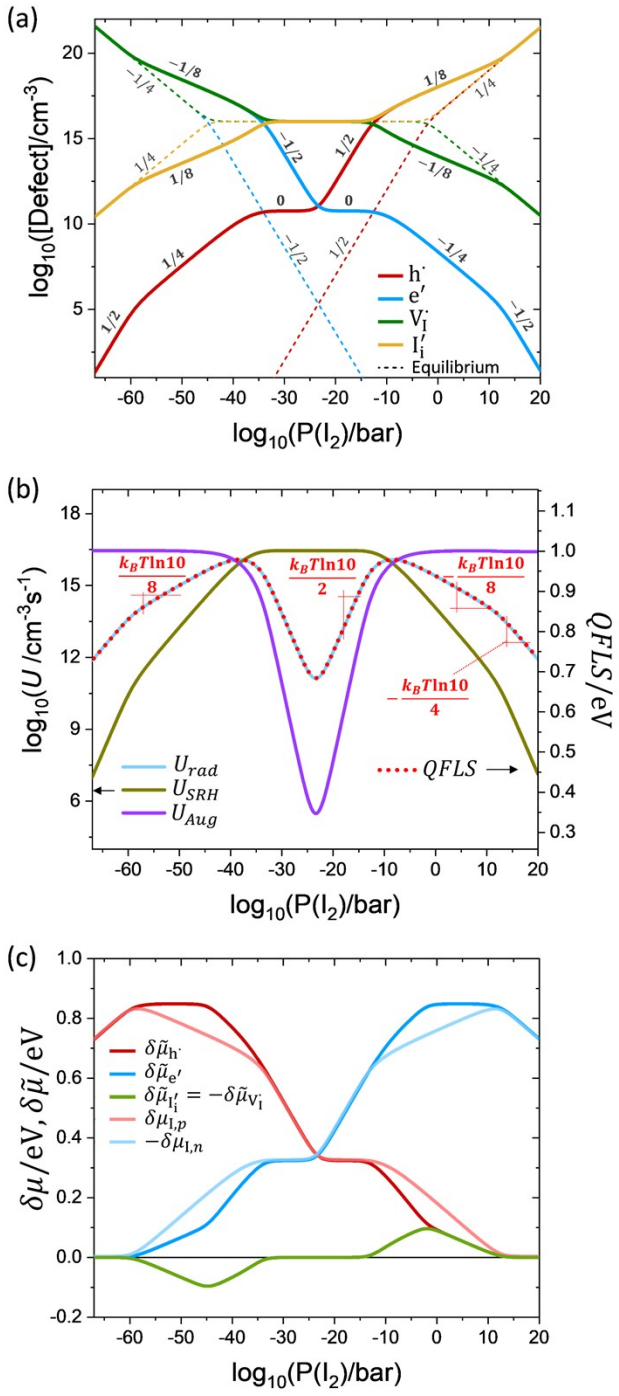

Figure S1. (a) Iodine partial pressure ($P(I_2)$) dependence of the steady-state electronic and ionic defect concentrations in MAPI at equilibrium and under light ($\sim 10^{-5}$ suns) for $\Gamma_{I,i} = 1$ plotted in a Kröger-Vink diagram· (b) Net recombination contributions and quasi-Fermi level splitting. (c) Changes in (quasi-)chemical and (quasi-)electrochemical potentials of all defects and of iodine.

Figure S1a and b show results from a calculation analogous to the one shown in Figure 3, but for a lower light intensity and for a wider $P(I_2)$ range. Figure S1c displays the corresponding changes in chemical and electrochemical potentials of all defects. From the discussion of Figure 3 in the main text, $\delta\tilde{\mu}_{V_I^\cdot} = -\delta\tilde{\mu}_{I_i^\cdot} = -\delta\tilde{\mu}_{I^-}$ ($\Delta\mu_F = 0$) at all $P(I_2)$, with $\delta\tilde{\mu}_{V_I^\cdot} \approx 0$ in the intrinsic region under light. In such region, the change in iodine quasi-chemical potentials can be expressed as $\delta\mu_{I,p} \approx \delta\mu_{h^\cdot}$ and $\delta\mu_{I,n} \approx \delta\mu_{e'}$, while in general both electronic and ionic contributions need to be taken into account ($\delta\mu_{I,p} = -\delta\tilde{\mu}_{V_I^\cdot} + \delta\tilde{\mu}_{h^\cdot}$ and $\delta\mu_{I,n} = -\delta\tilde{\mu}_{V_I^\cdot} - \delta\tilde{\mu}_{e'}$). Figure S1a shows that the concentration of both iodide defects and of holes (electrons) tend to the equilibrium value for very high (low) $P(I_2)$ values. Consistently, Figure S1c shows that $\delta\mu_{I,p}$ ($\delta\mu_{I,n}$) tends to 0 under such conditions, indicating that holes (electrons) essentially dominate the redox reactions and $\mu^*_{I,p}$ ($\mu^*_{I,n}$) matches $\frac{1}{2}\mu_{I_2,g}$.

Finally, the definition of $\tilde{\mu}^*_{e^-}$ under bias in the main text (see Figure 3c) is meaningful in the context of describing the free enthalpy change in the system per added electron (*i.e.* on increase in n or decrease in p). Unlike the quasi-electrochemical potentials $\tilde{\mu}^*_{e'}$ and $\tilde{\mu}^*_{h^\cdot}$, $\tilde{\mu}^*_{e^-}$ has no rigorous meaning when it comes to its relation with the occupation statistics of the electron and hole populations in the material's energy bands. Because anti-Frenkel disorder is at equilibrium in this example even under bias, $\tilde{\mu}^*_{I^-}$ maintains all the properties of $\tilde{\mu}_{I^-,eq}$.

4. One vs two redox-active ionic defects

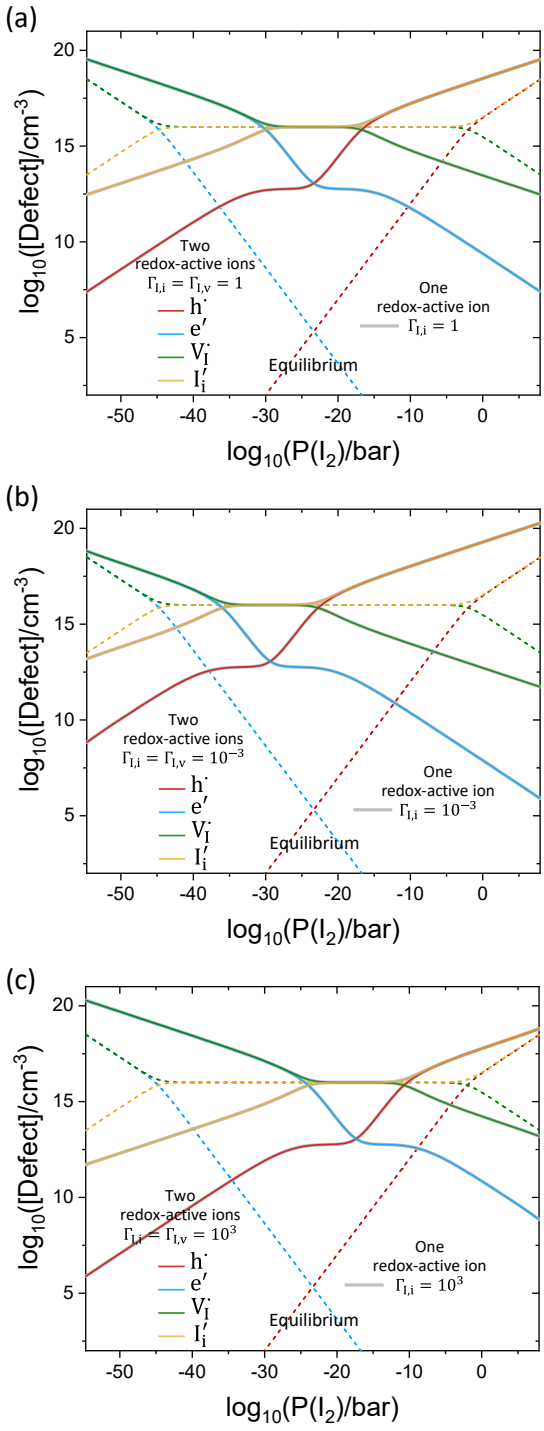

Figure S2. Defect concentrations obtained considering a one- (gray lines) or a two-redox-active mobile ion situation. For the latter, $\Gamma_{I,i} = \Gamma_{I,v}$ is considered. (a) $\Gamma_{I,i} = \Gamma_{I,v} = 1$ (b) $\Gamma_{I,i} = \Gamma_{I,v} = 10^{-3}$, (c) $\Gamma_{I,i} = \Gamma_{I,v} = 10^{3}$. Illumination of 10^{-3} suns is considered. A low value of $\Gamma_{p,i} = \Gamma_{n,v} = 10^{-2}$ is used.

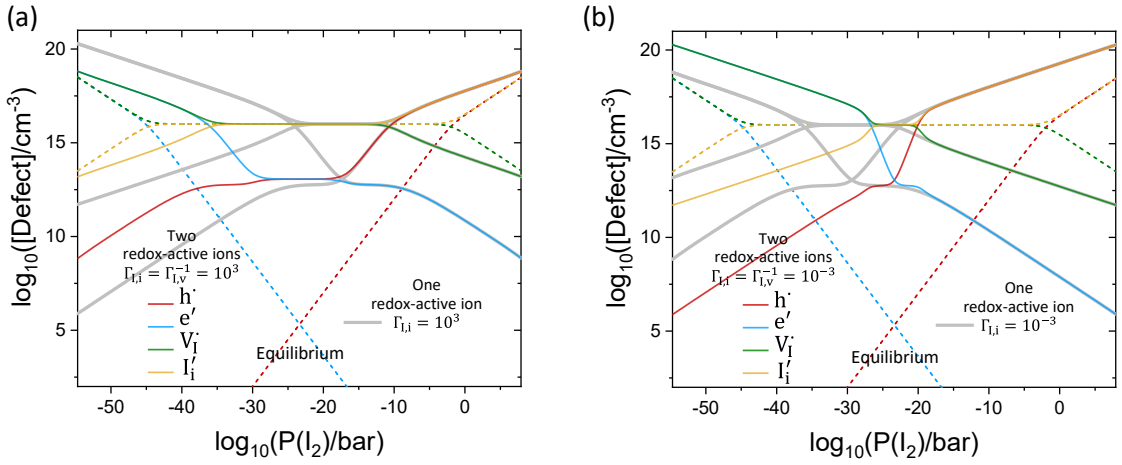

Figure S3. Defect concentrations obtained considering a one- (gray lines) or a two-redox-active mobile ion situation. The influence of $\Gamma_{I,i} \neq \Gamma_{I,v}$ is shown for (a) $\Gamma_{I,i} = 10^{3}, \Gamma_{I,v} = 10^{-3}$ and (b) $\Gamma_{I,i} = 10^{-3}, \Gamma_{I,v} = 10^{3}$. Illumination of 10^{-3} suns is considered.

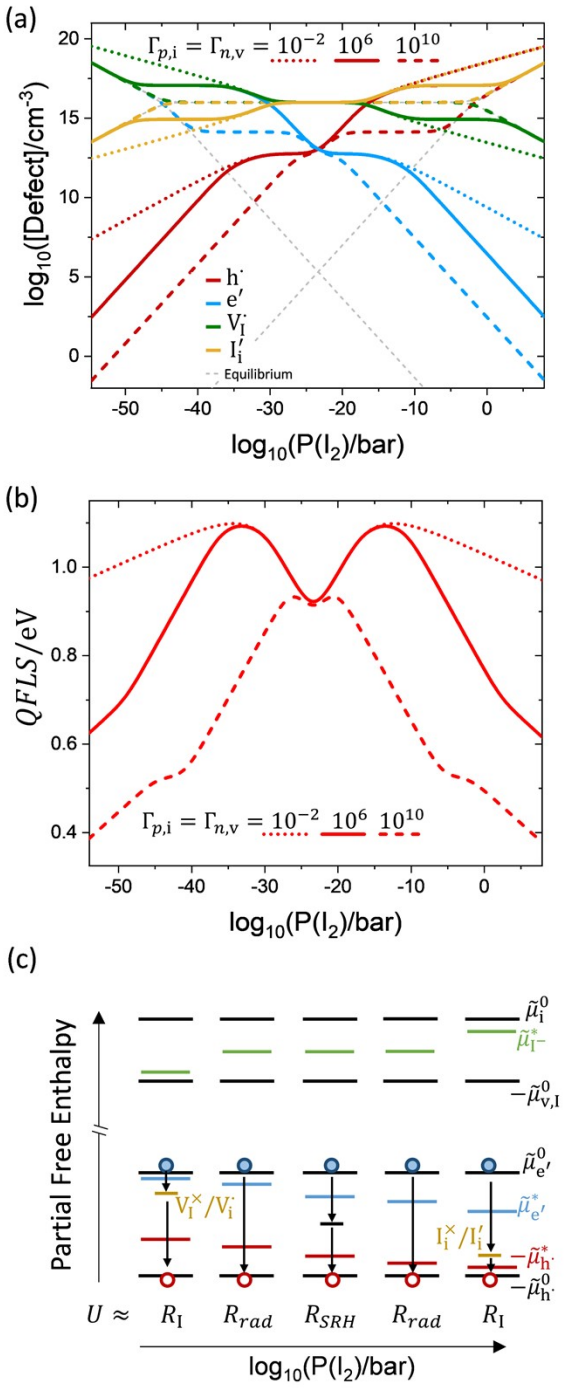

Figure S4. (a) Defect concentration and (b) $QFLS$ for a MAPI film calculated for $\Gamma_{p,i} = \Gamma_{n,v} = 10^{-2}$, 10^{6} and 10^{10} (corresponding to $\vec{k}_{p,i} = 2.1 \times 10^{-24}$, 2.1×10^{-16} and $2.1 \times 10^{-12}\ cm^3 s^{-1}$). Illumination of 10^{-3} suns and $\Gamma_{I,i} = \Gamma_{I,v} = 1$ are considered. (c) Generalized energy diagram showing the dominant recombination mechanisms for different $P(I_2)$ regions in (a) and (b) ($\Gamma_{p,i} = \Gamma_{n,v} = 10^{6}$ case). The $I_i^{\times}/I_i^{\cdot}$ and the $V_I^{\times}/V_I^{\cdot}$ energy levels are included (~ 0.3 eV from the valence band maximum and from the conduction band minimum, respectively).

Figure S4 shows that, when large values of $\Gamma_{p,i}$ and $\Gamma_{n,v}$ are used, the presence of the additional recombination pathway provided by the second defect leads to a similar trend as the one observed for Figure 4, but where a drop in $QFLS$ is observed not only for the high (recombination via $I_i^{\times}/I_i^{\cdot}$) but also for the low $P(I_2)$ range (recombination via $V_I^{\times}/V_I^{\cdot}$). This is illustrated schematically in Figure S4c.

5. Effect of solid-gas exchange kinetics on the ionic and electronic quasi-equilibrium

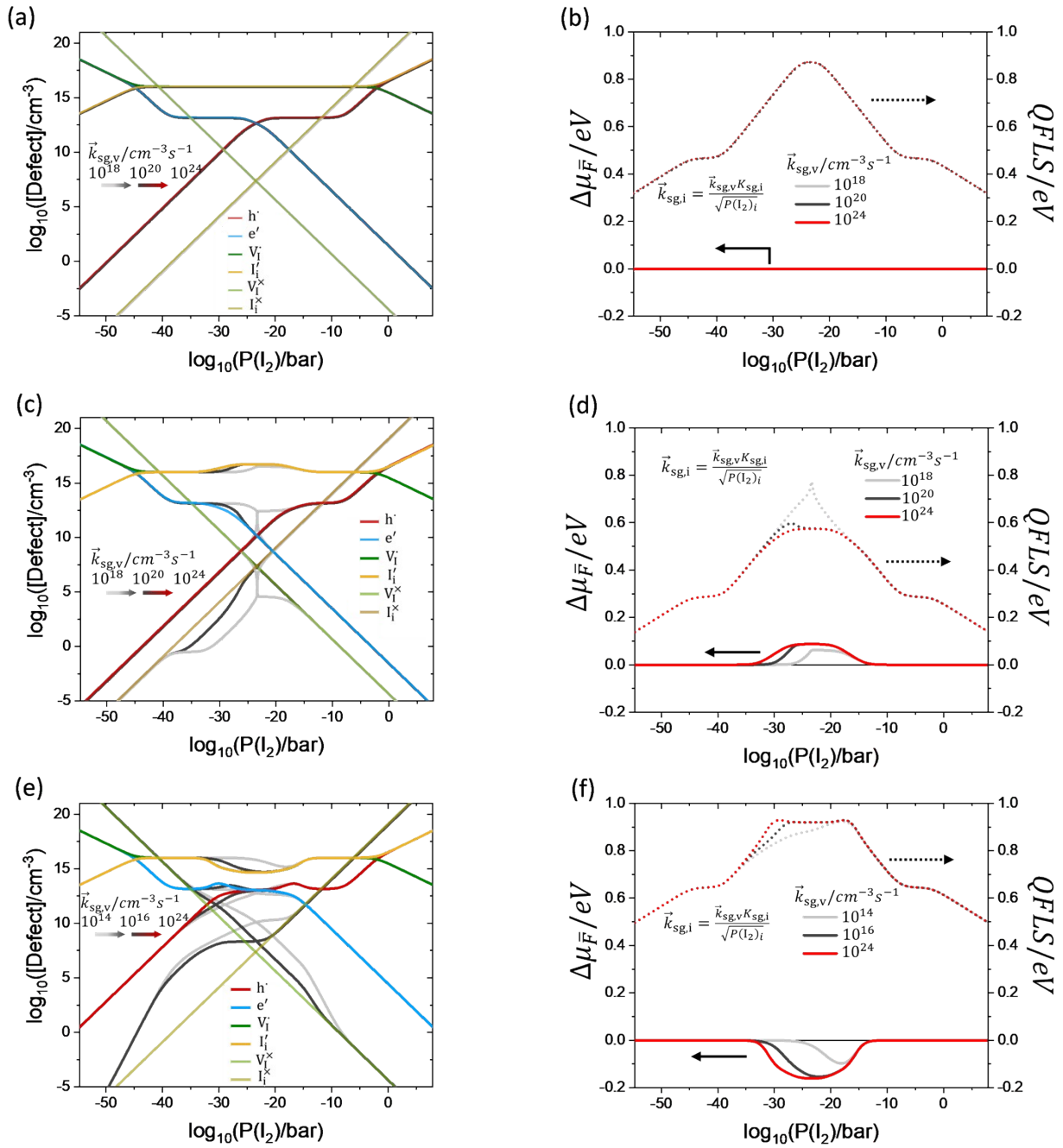

Figure S5. (left column) Defect concentrations and (right column) ionic ($\Delta\mu_F$) and electronic chemical potentials ($QFLS$) for different values of the rate constants controlling the solid-gas exchange. The values of the exchange rate constants $\vec{k}_{sg,v}$ and $\vec{k}_{sg,i}$ are varied together to ensure the same rate of solid-gas exchange mediated by iodine interstitials and iodine vacancies at equilibrium and at $P(I_2)_i$. (a, b) $\Gamma_{I,i} = \Gamma_{I,v} = 1$, (c, d) $\Gamma_{I,i} = 10^{-3}$,$\Gamma_{I,v} = 10^{3}$, (e, f) $\Gamma_{I,i} = 10^{3}$,$\Gamma_{I,v} = 10^{-3}$. Illumination of 10^{-3} suns is considered and $\Gamma_{p,i} = \Gamma_{n,v} = 10^{11}$. Deviation from the *sg-eq* behavior trend for the neutral ionic defect concentration highlights the kinetic limitations of the solid-gas exchange.

6. Effect of redox reaction kinetics on the ionic and electronic quasi-equilibrium

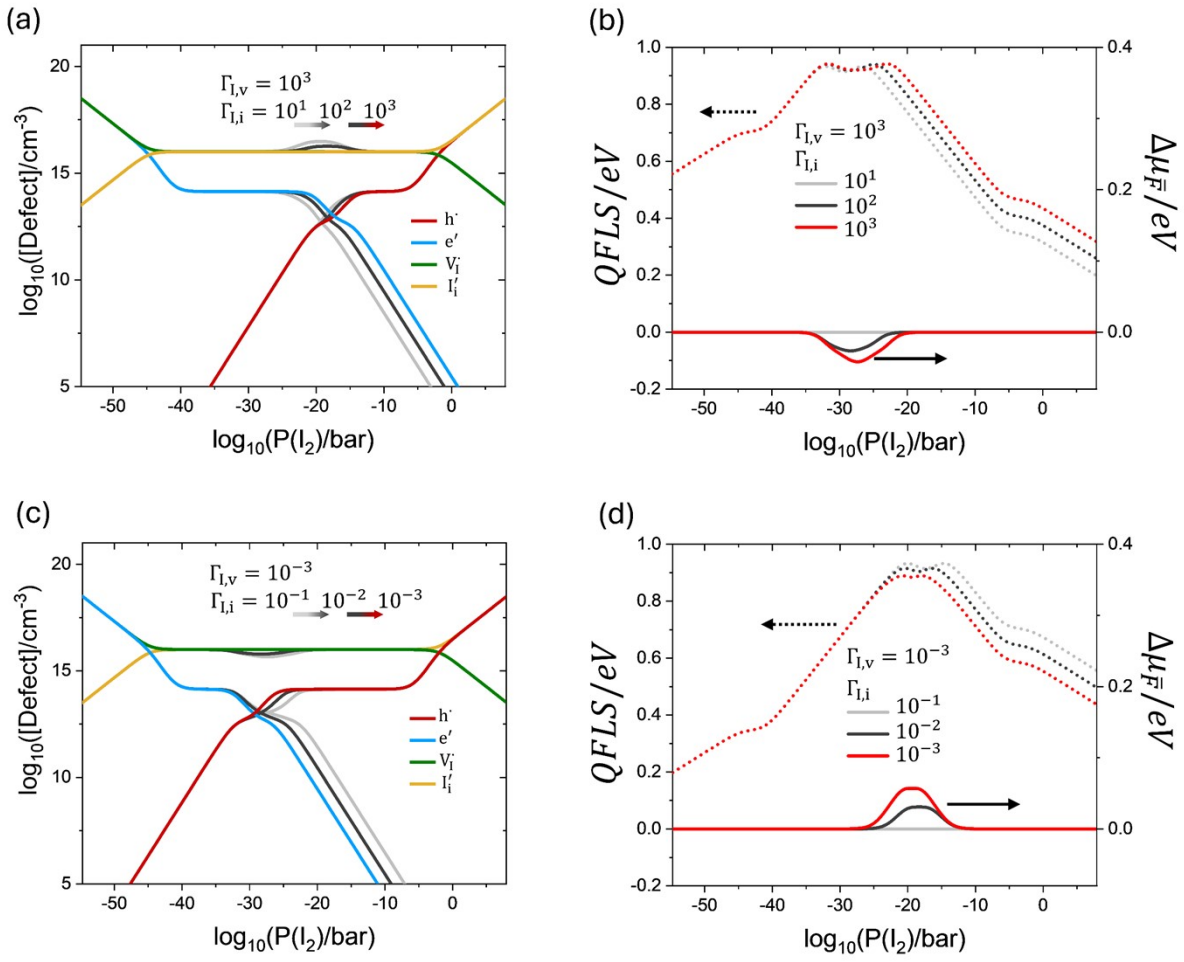

Figure S6. (left column) Defect concentrations and (right column) ionic ($\Delta\mu_{\bar{F}}$) and electronic chemical potentials ($QFLS$) for: (a, b) $\Gamma_{I,v} = 10^{3}$ (c, d) $\Gamma_{I,v} = 10^{-3}$ and varying values of $\Gamma_{I,i}$. Illumination of 10^{-3} suns is considered.

7. Electronic and ionic quasi-equilibrium in absence of immobile defect-mediated recombination

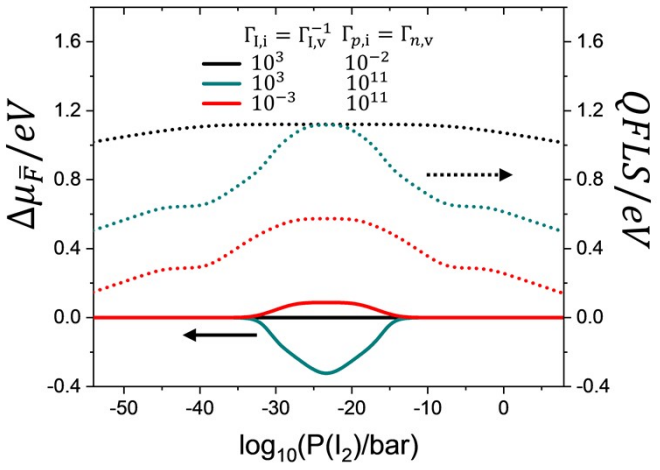

Figure S7. ionic ($\Delta\mu_{\bar{F}}$) and electronic chemical potentials ($QFLS$) for different input parameters. Illumination of 10^{-3} suns is considered. As no immobile trap-mediated SRH recombination is considered, when recombination via iodide defects is significant (large $\Gamma_{p,i} = \Gamma_{n,v}$), the $QFLS$ profile correlates with the density of anti-Frenkel defects. The latter scale exponentially with $\Delta\mu_{\bar{F}}$.

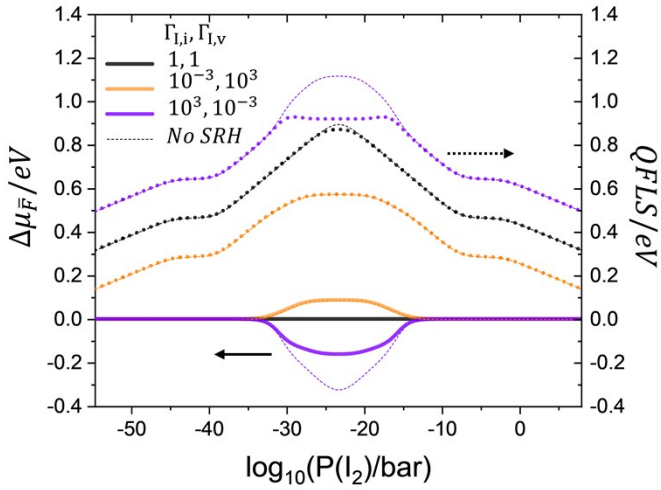

Figure S8. Data for the ionic ($\Delta\mu_{\bar{F}}$) and electronic chemical potentials ($QFLS$) shown in Figure 6a in the main text, compared with the analogous situation but without contribution from SRH recombination due to immobile defects.

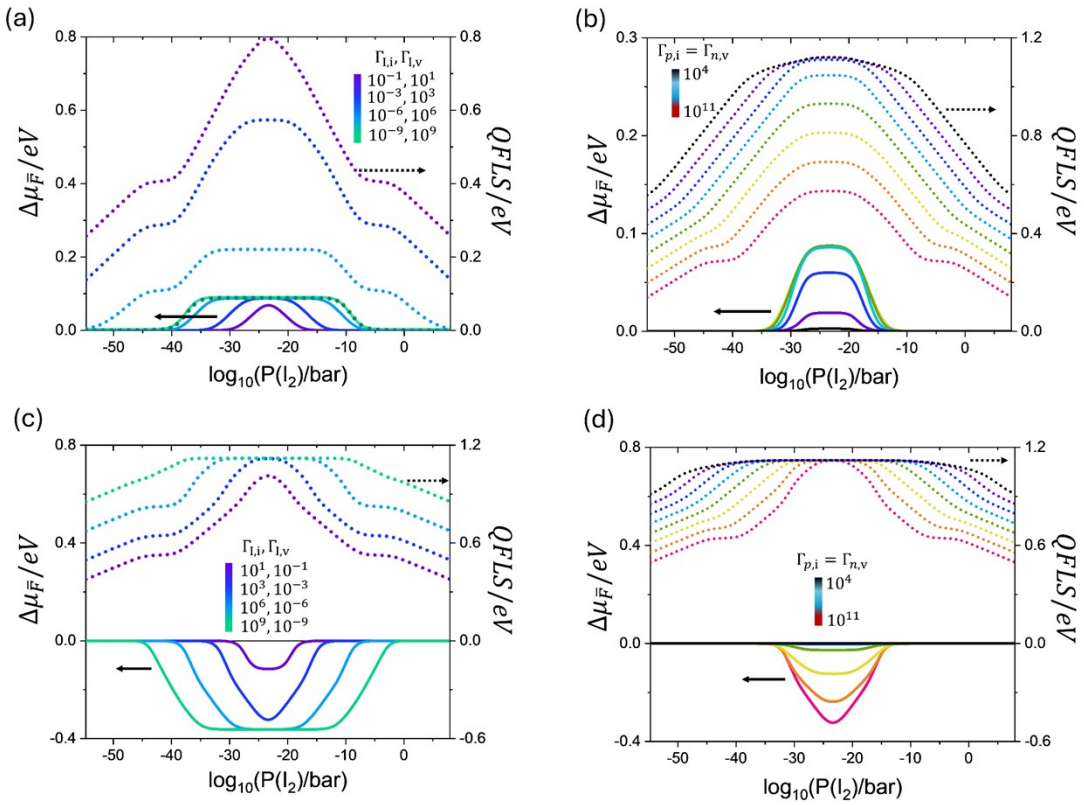

Figure S9. Dependence of the ionic ($\Delta\mu_{\bar{F}}$) and electronic ($QFLS$) change in chemical potential on the $\Gamma_{I,i}$, $\Gamma_{I,v}$, and $\Gamma_{p,i}$, $\Gamma_{n,v}$ parameters, as a function of $P(I_2)$. Trends for (a) increasing $h_{ion} > 0$ ($\Gamma_{p,i} = \Gamma_{n,v} = 10^{11}$), (b) increasing $\Gamma_{p,i} = \Gamma_{n,v}$ ($\Gamma_{I,i} = 10^{-3}$,$\Gamma_{I,v} = 10^{3}$), (c) decreasing $h_{ion} < 0$ ($\Gamma_{p,i} = \Gamma_{n,v} = 10^{11}$), (d) increasing $\Gamma_{p,i} = \Gamma_{n,v}$ ($\Gamma_{I,i} = 10^{3}$,$\Gamma_{I,v} = 10^{-3}$). All remaining parameters are the same as the ones used in Figure 3. $h_{ion} = \log_{10}\left(\frac{\Gamma_{I,v}}{\Gamma_{I,i}}\right)$. The data are obtained for a situation analogous to Figure 8, but with no contribution from SRH recombination due to immobile defects.

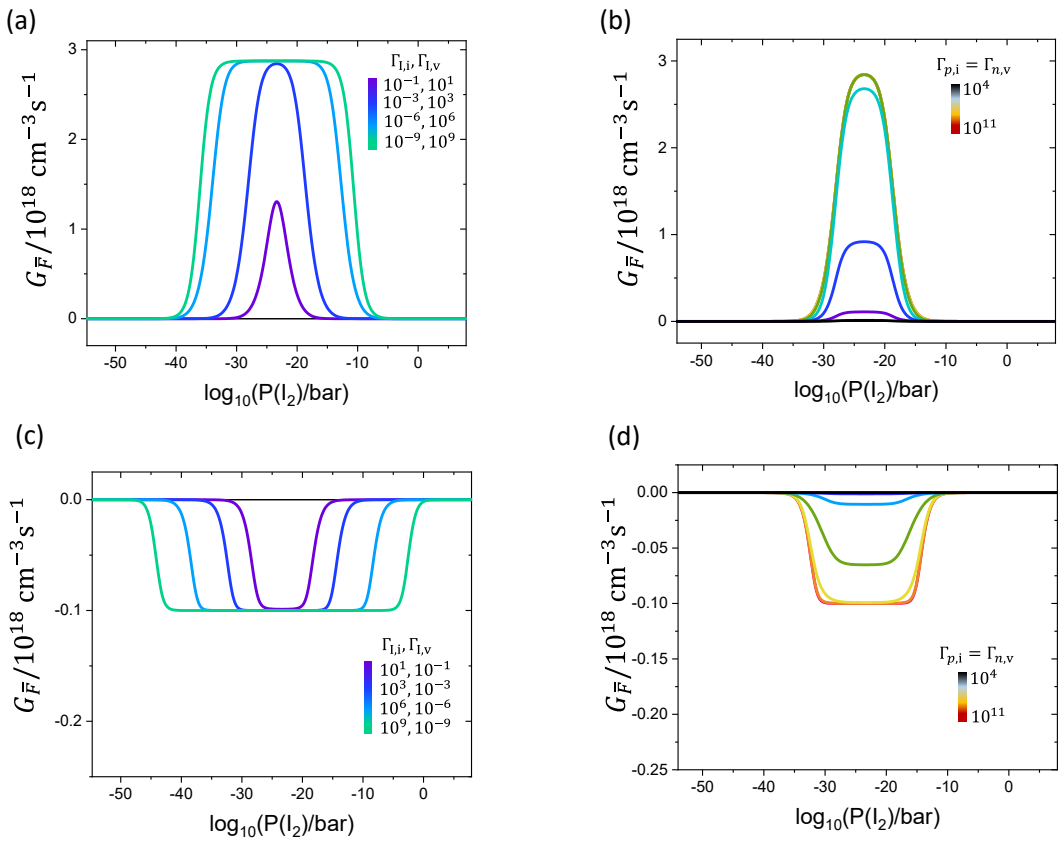

Figure S10. (a), (b), (c) and (d) show the effective ionic generation rates for the data displayed in Figure S9a, b, c and d, respectively.

8. Supporting References

1 T. Kirchartz, J. A. Márquez, M. Stolterfoht and T. Unold, *Advanced Energy Materials*, 2020, **10**, 1904134.

2 M. E. Ziffer, J. C. Mohammed and D. S. Ginger, *ACS Photonics*, 2016, **3**, 1060–1068.

3 D. A. Jacobs, C. M. Wolff, X.-Y. Chin, K. Artuk, C. Ballif and Q. Jeangros, *Energy Environ. Sci.*, 2022, **15**, 5324–5339.

4 D. Moia, M. Jung, Y.-R. Wang and J. Maier, *Phys. Chem. Chem. Phys.*, 2023, **25**, 13335–13350.

5 V. W. Lau, D. Klose, H. Kasap, F. Podjaski, M. Pignié, E. Reisner, G. Jeschke and B. V. Lotsch, *Angewandte Chemie*, 2017, **129**, 525–529.

6 J. Maier, *Physical Chemistry of Ionic Materials*, Wiley-VCH Verlag GmbH & Co. KGaA, 2nd edn., 2023.